Nonlinear Symmetry Breaking Induced by Third-Order Dispersion in Optical Fiber Cavities

François Leo,[1,2,*] Arnaud Mussot,[3] Pascal Kockaert,[1] Philippe Emplit,[1] Marc Haelterman,[1] and Majid Taki[3]

[1]*Service OPERA-photonique, Université libre de Bruxelles (U.L.B.), 50 Avenue F. D. Roosevelt, CP 194/5, B-1050 Bruxelles, Belgium*

[2]*Photonics Research Group, Department of Information Technology, Ghent University-IMEC, Ghent B-9000, Belgium*

[3]*PhLAM, Université de Lille 1, Bâtiment P5-bis, UMR CNRS/USTL 8523, F-59655 Villeneuve d'Ascq, France*

(Received 29 August 2012; published 5 March 2013)

We study analytically, numerically, and experimentally the nonlinear symmetry breaking induced by broken reflection symmetry in an optical fiber system. In particular, we investigate the modulation instability regime and reveal the key role of the third-order dispersion on the asymmetry in the spectrum of the dissipative structures. Our theory explains early observations, and the predictions are in excellent agreement with our experimental findings.

DOI: 10.1103/PhysRevLett.110.104103 PACS numbers: 05.45.−a, 42.65.Ky, 42.81.Qb

In the last decades there has been a tremendous amount of interest in the role of advection (drift) in pattern formation [1,2]. Its impact on nonlinear dynamical systems has been intensively studied in such diverse fields as hydrodynamics [3], plasma physics [4], traffic flow [5], and nonlinear optics [6], forming a highly multidisciplinary research area. Advection is modeled by odd term derivatives that break the reflection symmetry of the equation under study. The most studied consequence of advection is the classification of two different types of instabilities arising in such systems namely convective and absolute instabilities [7]. In the convective region, localized perturbations grow in a comoving frame but are drifted out of the system in the absence of a continuous source of noise. Observable patterns are consequently called noise sustained structures [8]. In the absolute region, however, such drifting perturbations grow with time at any spatial position and therefore affect the system everywhere. Here, we focus on another important consequence of advection on pattern formation in nonlinear systems, the asymmetry of the generated nonlinear solutions. This nonlinear symmetry breaking has been theoretically studied in the Ginzburg-Landau [9,10], the Swift-Hohenberg [11] and reaction-diffusion [12] equations. Experimental observations of these asymmetric solutions have been performed in Taylor-Couette flows [13], reaction-diffusion systems [14], and optical fiber resonators [15,16].

We propose, to the best of our knowledge, the first complete characterization (analytical, numerical, and experimental) of such nonlinear asymmetric solutions, providing a deeper understanding of the origin of the observed asymmetries. Our focus lies in the field of fiber optics, where the advection term (third-order derivative) naturally appears when the second-order dispersion of the fiber mode is small. By tuning that convective parameter, we evidence an unexpected resonancelike behaviour of the asymmetry. We believe this striking feature is not limited to our particular system, and our conclusions can be extended to nonlinear systems where an odd-order derivative strongly impacts the dynamics.

We consider the modulation instability regime of a nonlinear high finesse fiber resonator that is well described by the mean field Lugiato-Lefever equation [17]. We are interested in the region of low group velocity dispersion, where the third-order dispersion (TOD) has to be taken into account, breaking the reflection symmetry ($\tau \rightarrow -\tau$).

Nonlinear symmetry breaking induced by the TOD has recently attracted a lot of attention in fiber systems, both dissipative [16,18] and conservative [19]. However, there still lacks an analytical investigation allowing a better understanding of this asymmetry in the nonlinear regime. Here, we provide analytical expressions of the TOD induced asymmetry and compare them to experimental findings, showing excellent agreement.

We will first present the experimental results that have motivated our work. We will then present our analytical method and finally compare both with numerical simulations. Most experimental investigations of nonlinear dynamics in fiber cavities are conducted under pulsed pumping conditions [15,16] because of the high peak power available and because the stimulated Brillouin scattering threshold is strongly increased when using short pulses. While this solution has allowed us to experimentally investigate the dynamics of these systems, a quantitative comparison with analytical results and the simplest models is usually hard to achieve. Hence, based on a previously reported setup allowing the effective suppression of stimulated Brillouin scattering [20], our experiments were carried out with a continuous wave pump.

The experimental setup is depicted in Fig. 1. The cavity is mainly made of a 102-m-long dispersion-shifted fiber (DSF), a varying section of a standard single mode fiber (SMF), and a 90/10 input coupler. An intracavity isolator (60 dB) is used to avoid stimulated Brillouin scattering, and a piezoelectric stretcher connected to a proportional-integral-derivative controller allows for the active stabilization of the cavity length on the power of the first harmonic corresponding to a given detuning [20,21]. The nonlinear coefficient of the DSF is 2.6 $(\mathrm{W\ km})^{-1}$, and the

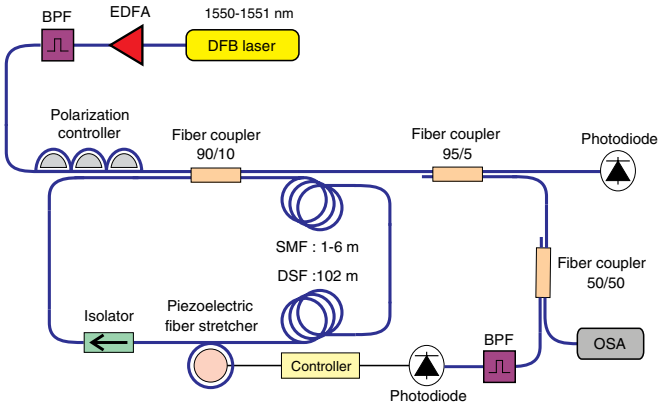

FIG. 1 (color online). Experimental setup: BPF denotes bandpass filter, EDFA denotes erbium-doped fiber amplifier, OSA denotes optical spectrum analyser.

total losses inside the cavity are 1.1 dB, which corresponds to a cavity finesse of 20. The cavity is pumped by a very narrow bandwidth distributed feedback (DFB) laser (1 kHz) amplified by an erbium-doped fiber amplifier. The experiment is performed as follows: The laser is amplified up to 202 mW, and the output power of the cavity is set to 70 mW. The total group velocity dispersion is then modified in two ways: (i) A coarse tuning is performed by removing SMF sections, and (ii) a fine-tuning is achieved by changing the wavelength of the pump, which is tunable over a 1-nm stretch around 1550.5 nm. We started with a SMF section of 6 m and cut back small samples of fiber corresponding to a total length of 5 m. This allows us to tune the second-order dispersion (SOD) from -1 to -0.1 ps^2/km. For each measurement, the output spectra have been averaged over 100 OSA sweeps in order to get clean traces.

As an example, four typical spectra are presented in Fig. 2. The mean group velocity dispersion in the top of the figure were retrieved from the relation giving the value of the most unstable frequency [17], which also corresponds to the repetition rate of the generated pulse train. Note that, as expected from standard theory, the shift of the most unstable frequency increases as $|\beta_2|$ (i.e., the SOD) decreases. Let us now focus on the asymmetry between the blue- and redshifted generated frequencies. The ratio between the fundamental frequencies is very low compared to the one observed for the second harmonics. For instance, more than 25 dB is observed in Fig. 2(b) for the second harmonic while there is only 1 dB for the first one. The SOD dependence of the ratios, R_{1h} and R_{2h}, is represented in blue dots in Figs. 3(a) and 3(b), respectively.

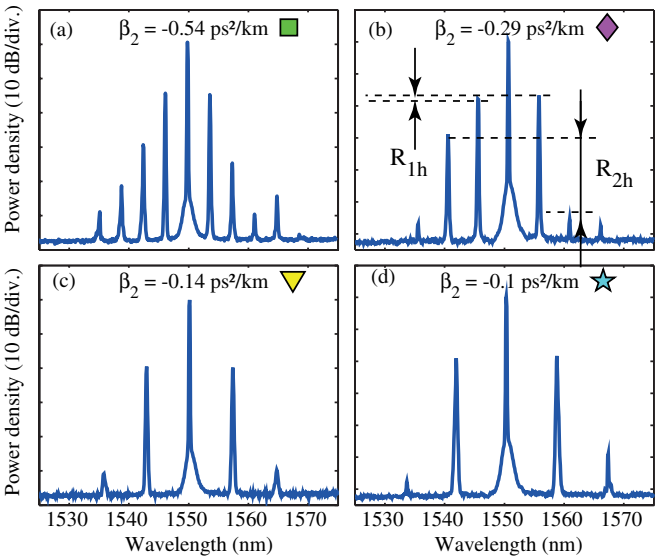

FIG. 2 (color online). Examples of experimental spectra for different values of the total group velocity dispersions. Each spectrum is averaged over 100 shots. From (a) to (d), the SOD decreases. R_{1h} remains close to 1 (i.e., 0 dB), while R_{2h} varies strongly.

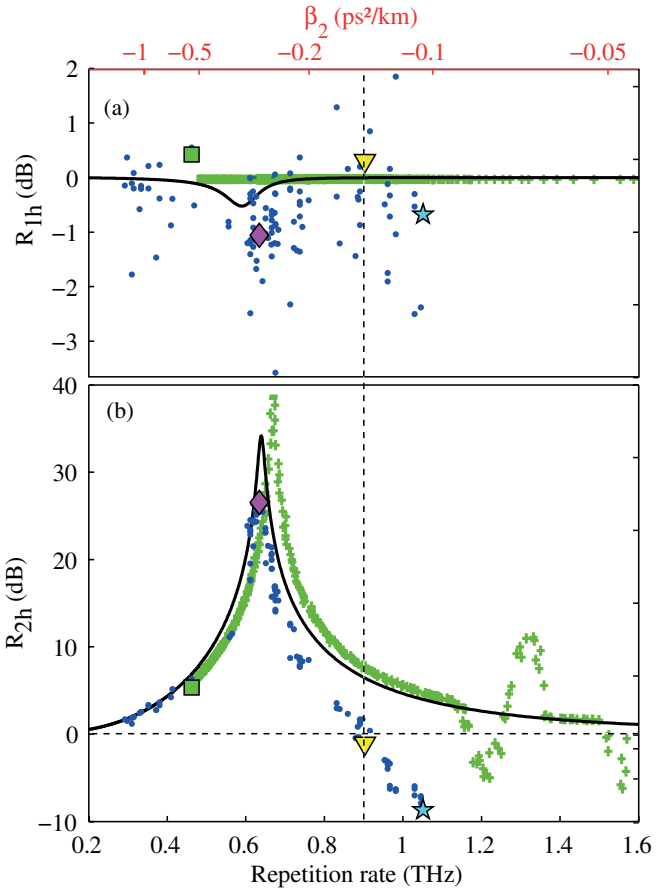

FIG. 3 (color online). Theoretical (black line), numerical (green crosses), and experimental (blue dots) evolution of the asymmetry of the first and second harmonics with the SOD as a function of either the repetition rate (bottom x axis) or of the SOD (top x axis). Parameters: $\beta_3 = 1.2^{-40}$ s^3/m, $\delta = 0.08$ ($\Delta = 0.5$), $\alpha = 0.16$, $L = 105$ m, and $P_{\text{in}} = |E_{\text{in}}|^2 = 202$ mW.

While we do not see a pattern emerging for the first harmonic asymmetry when working so close to the threshold, the curve depicting the asymmetry for the second harmonics clearly exhibits a huge resonance of nearly 30 dB around $\beta_2 = -0.29$ ps^2/km [Fig. 3(b)]. This remarkable spectral asymmetry of the modulated structures stems from the broken reflection symmetry induced by the third-order dispersion. Its occurrences in the spectrum have been experimentally observed in conservative [19] as well as dissipative [16,18] systems, and a full theoretical description of this behavior is a long standing issue. Indeed, this asymmetry cannot be described within the standard linear stability analysis. In order to explain and better understand this nonlinear behavior, a more complex analysis based on order parameter description is necessary to account for the impact of higher-order harmonics on the dynamics of the system above threshold [22]. The system under investigation depicted in Fig. 1 can be modeled by the extended nonlinear Schrödinger equation with boundary conditions. This leads to a set of two equations, usually referred to as the map equations (or mapping), that can be combined together by following the Lugiato-Lefever assumptions to obtain a single equation that models the dynamics of the cavity. This equation, known as the Lugiato-Lefever equation [17], has proven relevant for describing weakly nonlinear dynamics in cavities [23]. It reads

$$\frac{\partial \psi(t',\tau')}{\partial t'} = \left[-1 + i[|\psi(t',\tau')|^2 - \Delta] - i\beta_2 \frac{\partial^2}{\partial \tau'^2} + B_3 \frac{\partial^3}{\partial \tau'^3}\right]\psi(t',\tau') + S, \quad (1)$$

where $t' = \alpha t/t_R$, with t the real time and t_R the round trip time, $\tau' = \tau\sqrt{2\alpha/L}$, $\psi = E\sqrt{\gamma L/\alpha}$, $S = E_{\text{in}}\sqrt{\gamma L\theta/\alpha^3}$, $B_3 = \beta_3\sqrt{2\alpha/9L}$, and $\Delta = \delta/\alpha$, with the following physical parameters, α the linear losses of the cavity, θ the transmission coefficient of the cavity, γ the nonlinear coefficient of the fiber, L the cavity length, β_2 the SOD, β_3 the TOD, δ the cavity phase detuning, E the intracavity electric field, and E_{in} the electric pump field. Both convective and absolute instabilities have been recently reported for the steady-state solution E_s of the stationary form of (1): $S = [1 + i(\Delta - I_s)]E_s$, where $I_s = |E_s|^2$ [16]. Note that, in the case of a cw pump, there is no appreciate difference between absolute and convective regions for the accessible experimental values of the parameters. Here, we devote our attention to the case $\Delta < 41/30$ and $\beta_2 < 0$, for which fiber cavities exhibit a supercritical bifurcation at $I_s = 1$ [17]. This is the threshold at which stationary homogeneous solutions become unstable. Under such conditions, the system evolves toward modulated solutions characterized by a frequency $\Omega_c = \sqrt{(\Delta - 2)/\beta_2}$ and a wave vector $\kappa_c = -B_3\Omega_c^3$. Limited to five spectral modes, these solutions read

$$\psi_s(t,\tau) = D + A^+ e^{i(\Omega_c\tau + \kappa_c t)} + A^- e^{-i(\Omega_c\tau + \kappa_c t)} + C^+ e^{2i(\Omega_c\tau + \kappa_c t)} + C^- e^{-2i(\Omega_c\tau + \kappa_c t)}. \quad (2)$$

Within our model, the nonlinear symmetry breaking corresponds to $A^+ \neq A^-$ and $C^+ \neq C^-$ or, equivalently, to $R_{1h} = |A^-|^2/|A^+|^2 \neq 1$ and $R_{2h} = |C^-|^2/|C^+|^2 \neq 1$. The coefficients R_{1h} and R_{2h} characterize, respectively, the asymmetry of the first and the second harmonics. In order to find analytical expressions for R_{1h} and R_{2h} and explain our experimental observations, we perform a multiscale analysis similar to the one developed in Ref. [9]. First, we expand the variables in the small parameter ε, defined as $\varepsilon^2 = I_s - 1$, that is the distance from the instability threshold. The envelope of the electric field is rewritten in terms of the amplitudes a_k, defined by $E = E_s + \varepsilon a_1 + \varepsilon^2 a_2 + \varepsilon^3 a_3 + \cdots$. Following the approach of Ref. [22] and taking into account the gain spectrum of the instability [23], we introduce the new times: $T_0 = t$, $T_1 = \varepsilon t$, $T_2 = \varepsilon^2 t$, $\tau_0 = \tau$, and $\tau_1 = \varepsilon\tau$ so that the corresponding temporal derivatives become $\partial_t = \partial_{T_0} + \varepsilon\partial_{T_1} + \varepsilon^2\partial_{T_2}$ and $\partial_\tau = \partial_{\tau_0} + \varepsilon\partial_{\tau_1}$. We then assume that the amplitudes a_k are the sum of quasimonochromatic waves written in the form $a_1 = K(A_1 e^{i(\Omega_c\tau_0 + \kappa_c T_0)} + A_1^* e^{-i(\Omega_c\tau_0 + \kappa_c T_0)})$, and $a_k = D_k + A_k^+ e^{i(\Omega_c\tau_0 + \kappa_c T_0)} + A_k^- e^{-i(\Omega_c\tau_0 + \kappa_c T_0)} + C_k^+ e^{2i(\Omega_c\tau_0 + \kappa_c T_0)} + C_k^- e^{-2i(\Omega_c\tau_0 + \kappa_c T_0)}$, with $k = 2, 3$. The form of a_1 is justified by the fact that, right above the instability threshold, the gain is only positive in the vicinity of $\Omega \approx \pm\Omega_c$, while, for the second- and third-order corrections, contributions at 0 and $\pm 2\Omega_c$ appear because of the nonlinear interactions. By substitution of the above expansions in Eq. (1), we obtain a hierarchy of equations for the successive orders of ε. Solving the system up to the third order, we obtain analytical expressions of the asymmetries for the first and second harmonics [24]. They read

$$R_{1h} = \frac{|A^-|^2}{|A^+|^2} = 1 + H\frac{4M}{(1 - MH)^2 + N^2}, \quad (3)$$

$$R_{2h} = \frac{|C^-|^2}{|C^+|^2} = 1 - H\frac{12 - 20G}{2 - 6(G - H) + 5(G - H)^2}, \quad (4)$$

with

$$M = \frac{1 - Is}{d_1}\frac{12 - 20G}{(G^2 - H^2)^2 + 4H^2}, \quad (5)$$

$$N = Is - 1 + \frac{1 - Is}{d_1}\left(3 + 12\frac{7G + 9}{G^2} + \frac{(6 - 10G)(G^2 - H^2)}{(G^2 - H^2)^2 + 4H^2}\right), \quad (6)$$

$$d_1 = 24\frac{2G + 3}{G^2} + 4\frac{G^2(1 - 2G) + H^2(2G - 3)}{(G^2 - H^2)^2 + 4H^2}, \quad (7)$$

$$G = 3(\Delta - 2), \quad (8)$$

$$H = 6\kappa_c = -6B_3\Omega_c^3. \quad (9)$$

Let us emphasize the role of the dimensionless H parameter, proportional to the ratio $\beta_3/\beta_2^{3/2}$. We can see from Eqs. (3) and (4) that the asymmetry on both harmonics cancel as expected when $H = 0$, i.e., when $\beta_3 = 0$. The theoretical dependence of both R_{1h} and R_{2h} on β_2 are presented in Fig. 3 and compared with our experimental results.

On this figure, we first see that the theoretical asymmetry R_{1h} [Fig. 3(a)] is very weak, which explains the difficulty to observe it in experiments. Second, we observe a very good agreement between the analytical model and the experimental results for the asymmetry R_{2h}. In particular, the position of the resonance is very well reproduced by our theoretical analysis. The difference in the strength of the asymmetry of the first and second harmonics can be understood from the different steps of the multiscale analysis. The first order of the calculation is equivalent to the linear stability analysis, generating two sidebands at the frequency of maximum gain Ω_c. Their amplitudes are the same as they are both on resonance. On the second order, nonlinear wave mixing of those waves and the pump generates the second harmonic sidebands. The different resonating conditions induced by the TOD lead to different amplitudes for the Stokes (long wavelength side) and anti-Stokes wave (short wavelength side). Finally, at the third order, the nonlinear mixing of the asymmetric second harmonic waves with the pump lead to a small asymmetric correction on the first harmonic. This shows that both the first and second harmonic asymmetries come from the resonating conditions of the second harmonic.

The comparison of our analytical and experimental results shows a big discrepancy for group velocity dispersions lower than -0.2 ps^2/km. We attribute this to the limited validity of the mean-field equation (1). Indeed, in the frame of the mean-field model, the system is described by a single Lorentzian peak. This requires that all contributions to the accumulated phase per round trip must be much smaller than the free spectral range. But, for SODs lower than -0.2 ps^2/km, the TOD contribution to the accumulated phase of the second harmonics becomes of the same order of magnitude as the free spectral range. As these sidebands reach the nearest resonance, their behavior is not described correctly by the mean-field model anymore.

The redshifted second harmonic is the first to reach the nearest resonance, while the corresponding blueshifted component is in between resonances. This induces a reversal of the asymmetry that cannot be seen within the mean-field model. In order to confirm this phenomenon, we compared our results to numerical simulations performed on the map equations. These simulations have been performed with a slightly higher pump power (230 mW) that corresponds to the threshold in numerical simulations. Note that output spectra have been denoised by using Savitzky-Golay smoothing filters. They confirm our explanations and show clear secondary resonances for the second harmonics, as can be seen in Fig. 3(b) (green crosses).

Unfortunately, we were experimentally limited to SOD lower than -0.1 ps^2/km and couldn't observe the secondary resonances as (i) the stabilization of our device becomes very hard to achieve and (ii) the power of the second harmonics becomes too low to be measured.

In summary, we studied analytically, numerically and experimentally the TOD induced nonlinear symmetry breaking of the modulation instability process in optical fiber resonators. We give new insight on the physical origin of the asymmetry on both the first and second harmonics in the vicinity of the threshold. Our analytical predictions are in excellent agreement with the experimental findings except for low group velocity dispersion where we show that the mean-field approximation is no longer valid. This unexpected difference between the analytical and experimental results is well described by numerical solutions obtained by integrating the original full mapping model of the cavity instead of the reduced Lugiato-Lefever equation. It is worth noting that the Lugiato-Lefever equation (1), which is a particular realization of a forced complex Ginzburg-Landau equation [25], models a broad area of physical systems ranging from long Josephson junctions to rf-driven plasma [26]. Our work can then contribute to a further understanding of nonlinear symmetry breaking in these fields and may shed light on experimental results of dissipative structures displaying strong asymmetries (see, e.g., Refs. [13,27]).

This work is supported by the Belgian Science Policy Office (BelSPO) under Grant No. IAP 7-35, French Ministry of Higher Education and Research, the Nord-Pas de Calais Regional Council, and FEDER through the "Contrat de Projets Etat Région (CPER) 2007-2013," the "Campus Intelligence Ambiante" (CIA), and the French Ministry of Research. The authors would like to thank Bendix Schneider and Etienne Averlant for precious help in the laboratory.

*francois.leo@ulb.ac.be

[1] M. Cross and P. Hohenberg, Rev. Mod. Phys. **65**, 851 (1993).
[2] J. D. Murray, *Mathematical Biology* (Springer, Berlin, 1993).
[3] P. Huerre and P. A. Monkewitz, Annu. Rev. Fluid Mech. **22**, 473 (1990); A. Couairon and J. M. Chomaz, Phys. Rev. Lett. **79**, 2666 (1997); H. R. Brand, R. J. Deissler, and G. Ahlers, Phys. Rev. A **43**, 4262 (1991); P. Buchel and M. Lucke, Phys. Rev. E **61**, 3793 (2000).
[4] R. J. Briggs, *Electron-Stream Interaction with Plasmas* (MIT Press, Cambridge, MA, 1964).
[5] N. Mitarai and H. Nakanishi, Phys. Rev. Lett. **85**, 1766 (2000).

[6] G. Izus, M. Santagiustina, M. San Miguel, and P. Colet, J. Opt. Soc. Am. B **16**, 1592 (1999); H. Ward, M. N. Ouarzazi, M. Taki, and P. Glorieux, Phys. Rev. E **63**, 016604 (2000).
[7] J. M. Chomaz, Phys. Rev. Lett. **69**, 1931 (1992).
[8] M. Santagiustina, P. Colet, M. San Miguel, and D. Walgraef, Phys. Rev. Lett. **79**, 3633 (1997); E. Louvergneaux, C. Szwaj, G. Agez, P. Glorieux, and M. Taki, Phys. Rev. Lett. **92**, 043901 (2004).
[9] R. Zambrini, M. San Miguel, C. Durniak, and M. Taki, Phys. Rev. E **72**, 025603 (2005).
[10] R. J. Deissler, J. Stat. Phys. **40**, 371 (1985); S. M. Tobias, M. R. E. Proctor, and E. Knobloch, Physica (Amsterdam) **113D**, 43 (1998).
[11] J. Burke, S. M. Houghton, and E. Knobloch, Phys. Rev. E **80**, 036202 (2009); C. Kharif, E. N. Pelinovskii, and A. Slunyaev, *Rogue Waves in the Ocean* (*Springer-Verlag*, Berlin, 2009), Chap. 4 and references therein.
[12] S. P. Kuznetsov and E. Mosekilde, J. Chem. Phys. **106**, 7609 (1997); P. Andresen, M. Bache, E. Mosekilde, G. Dewel, and P. Borckmanns, Phys. Rev. E **60**, 297 (1999); B. von Haeften and G. Izus, Phys. Rev. E **67**, 056207 (2003).
[13] K. L. Babcock, G. Ahlers, and D. S. Cannell, Phys. Rev. Lett. **67**, 3388 (1991).
[14] M. Kaern and M. Menzinger, Phys. Rev. E **60**, R3471 (1999).
[15] S. Coen, M. Tlidi, P. Emplit, and M. Haelterman, Phys. Rev. Lett. **83**, 2328 (1999).
[16] A. Mussot, E. Louvergneaux, N. Akhmediev, F. Reynaud, L. Delage, and M. Taki, Phys. Rev. Lett. **101**, 113904 (2008).
[17] L. A. Lugiato and R. Lefever, Phys. Rev. Lett. **58**, 2209 (1987).
[18] S. Martin-Lopez, P. Corredera, and M. Gonzalez-Herraez, Opt. Express **17**, 12 785 (2009).
[19] M. Droques, B. Barviau, A. Kudlinski, M. Taki, A. Boucon, T. Sylvestre, and A. Mussot, Opt. Lett. **36**, 1359 (2011); M. Erkintalo, Y. Q. Xu, S. G. Murdoch, J. M. Dudley, and G. Genty, Phys. Rev. Lett. **109**, 223904 (2012).
[20] S. Coen and M. Haelterman, Opt. Lett. **26**, 39 (2001).
[21] F. Leo, S. Coen, P. Kockaert, S.-P. Gorza, P. Emplit, and M. Haelterman, Nat. Photonics **4**, 471 (2010).
[22] P. Manneville, *Instabilities, Chaos and Turbulence* (*Imperial College Press*, London, 1994).
[23] M. Haelterman, S. Trillo, and S. Wabnitz, Opt. Commun. **91**, 401 (1992).
[24] Note that the τ expansion allows for the calculation of all unstable modes. As shown in Eq. (2), here we only consider the mode with positive gain at the instability's threshold.
[25] P. Coullet and K. Emilsson, Physica (Amsterdam) **61D**, 119 (1992).
[26] I. V. Barashenkov and Y. S. Smirnov, Phys. Rev. E **54**, 5707 (1996).
[27] C. R. Nugent, W. M. Quarles, and T. H. Solomon, Phys. Rev. Lett. **93**, 218301 (2004).